



HAL
open science

Homochiral vs. heterochiral sodium core dimers of tartaric acid esters: A mass spectrometry and vibrational spectroscopy study

Katia Le Barbu-Debus, Debora Scuderi, Valéria Lepère, Anne Zehnacker

► **To cite this version:**

Katia Le Barbu-Debus, Debora Scuderi, Valéria Lepère, Anne Zehnacker. Homochiral vs. heterochiral sodium core dimers of tartaric acid esters: A mass spectrometry and vibrational spectroscopy study. *Journal of Molecular Structure*, 2020, 1205, pp.127583. 10.1016/j.molstruc.2019.127583 . hal-02441869

HAL Id: hal-02441869

<https://hal.science/hal-02441869>

Submitted on 16 Jan 2020

HAL is a multi-disciplinary open access archive for the deposit and dissemination of scientific research documents, whether they are published or not. The documents may come from teaching and research institutions in France or abroad, or from public or private research centers.

L'archive ouverte pluridisciplinaire **HAL**, est destinée au dépôt et à la diffusion de documents scientifiques de niveau recherche, publiés ou non, émanant des établissements d'enseignement et de recherche français ou étrangers, des laboratoires publics ou privés.

Homochiral vs. Heterochiral Sodium Core Dimers of Tartaric Acid Esters: a Mass Spectrometry and Vibrational Spectroscopy Study

Katia Le Barbu-Debus,^a Debora Scuderi,^b Valeria Lepère,^a Anne Zehnacker^{*a}

a) Institut des Sciences Moléculaires d'Orsay (ISMO), CNRS, Univ. Paris-Sud, Université Paris-Saclay, F-91405 Orsay, France

b) Univ. Paris-Sud, Laboratoire de Chimie Physique, UMR8000, and CNRS, Orsay, F-91405 France

*e-mail anne.zehnacker-rentien@u-psud.fr

Abstract

The mixed sodium core dimers of dimethyl-L-tartrate (Lmt) and the two enantiomers of diisopropyl tartrate (Lipt and Dipt) are studied by mass spectrometry coupled with laser vibrational spectroscopy. Infra-Red Multiple Photon Dissociation (IRMPD) spectra of the two diastereomer sodium-core dimers, namely, LmtLiptNa⁺ and LmtDiptNa⁺, are identical in the fingerprint region but show a slight difference in the OH stretch region. Comparison to *ab initio* calculations indicates that the formed complexes probably reflect the structures pre-existing in solution. The difference between LmtLiptNa⁺ and LmtDiptNa⁺ arises from the presence of an additional Na⁺...O interactions in the homochiral complex. The two complexes also differ in the strength and nature of the OH...OC hydrogen bond.

Highlights:

- Sodium ion-core dimers of tartaric acid esters are studied by mass spectrometry and laser spectroscopy
- Infra-red Multiple photon spectroscopy coupled with quantum chemical calculations aim at explaining the chirality effects observed in these systems.

- Infra-red spectroscopy shows that the dimer with two monomers of identical absolute configuration possesses one more hydrogen bond relative to the heterochiral dimer.

Introduction

Mass spectrometry is widely used for the analysis of biological systems, in particular proteins.¹ One of its limitations is that, as an achiral probe, mass spectrometry is blind to chirality and is unable to differentiate enantiomers. A widely developed approach is to associate mass spectrometry to a chirality-sensitive separation stage, most of the time chromatography,²⁻³ sometimes ion mobility.⁴⁻⁵ On the other hand, formation of diastereomeric complexes have proven especially efficient for chiral analysis using mass spectrometry.⁶ Different binding energies between the enantiomers manifest themselves by different abundances in a single-stage MS spectrum.⁷ Isotope labelling is mandatory for differentiating the two enantiomers, whose masses are identical otherwise. Diastereomer complexes may also show different ion-molecule reaction, for example exchange reactions involving chiral host-guest complexes.⁸⁻¹⁰ Lastly, experiments based on cluster ion dissociations are a powerful tool for chiral analysis. These experiments rest on the comparison between the collision-induced dissociation efficiency of diastereomer complexes, both in a single-collision regime¹¹ or in a multiple collision regime under ion trap conditions.¹²⁻¹⁷ Tandem mass spectrometry experiments based on the kinetic method allow quantifying chirality effects.¹⁸⁻¹⁹ The enantioselectivity in the dissociation is related to different binding energies or different barriers to dissociation between enantiomers,¹⁴ or to entropic effects.²⁰ The differences in the binding pattern of the diastereomers also manifests itself in their UV photodissociation spectrum or UV photodissociation pathways.^{15, 21-22} Because they can be directly compared to quantum chemical calculations, IR spectra are also a good diagnostic of stereo-selective interactions in diastereomer ions.²³⁻²⁶ Tartaric acid and its derivatives play an important role in asymmetric chemistry. Besides their involvement in the discovery of molecular chirality by Pasteur,²⁷ they are used as eluents in the separation of enantiomers by chromatography.²⁸ Their chirality recognition properties have been studied also in the gas phase by mass spectrometry experiments.²⁹⁻³⁰ Protonated dimethyl tartrate dimers formed by chemical ionization were the first study of chiral recognition by mass spectrometry experiments.³¹ The mass spectrum of a mixture of diisopropyl-d₀ D-tartrate and diisopropyl-d₆ L-tartrate shows anomalously weak intensity of the peak corresponding to the diisopropyl-d₀ D-tartrate:diisopropyl-d₆ L-tartrate protonated dimer

(the *meso* ion), which indicates homochiral preference.³¹ Nikolaev *et al.* conducted a systematic study of chirality effects in protonated dimers and alkali-ion core dimers of dimethyltartrates.³²⁻³³ They observed that the sign as well as the magnitude of the observed chirality effect depend on the size of the cluster and the core ion. In particular, they observe a large chirality effect in the cluster distribution for several protonated cluster sizes formed by chemical ionization, as observed by Fales and Wright for the dimer.³¹ In contrast, the distribution of alkali-core dimers formed by ion-molecule reaction in the gas phase was identical for both homo and heterochiral dimers. These results obtained by chemical ionisation are in sharp contrast to those obtained when the ion-core, for example sodium-core dimer, is electrosprayed from a solution. The proposed explanations rest on displacement of the proton by the alkali ion in the final stage of desolvation, although enantioselective decomposition from trimers could not be excluded.³²⁻³³

Direct structural data are scarce. Tonner *et al.* have studied the structure of the isolated dianion of tartaric acid by Infra-Red Multiple Photon Dissociation (IRMPD) under ion trap conditions, as a model for studying the stability of dianions, and its complex with sodium. They have compared the binding pattern of sodium with the *threo* tartaric acid dianion to that observed for the *meso* form.³⁴ The *threo* tartrate anion is more stable than the *meso* form, whether isolated or complexed with sodium. For both systems, Na⁺ strongly interacts with the negatively charged carboxylate oxygen, with however slightly different interaction distances and binding pattern in the *threo* or *meso* tartrate, which are apparent in the vibrational spectra. Esters of tartaric acid have been studied too, in particular their titanium complexes, because of their role as catalysts.³⁵ The IRMPD spectrum of the (methyl-tartrate:dimethyl-tartrate Ti) complex indicates that the interaction between the titanium ion and the tartrate involves the carboxylate.

In this work, we revisit the question of homochiral preference in alkali-ion core tartaric acid ester dimers produced by electrospray ionisation. Na⁺ was chosen in this study because for the sake of comparison with the previous studies mentioned above and because its small size makes it amenable for calculations. The molecules under study are shown in Scheme 1 and noted in short dimethyl L-tartrate (Lmt) and diisopropyl D/L-tartrate (Lipt/Dipt). Our goal is to compare the sodium core dimers having molecules of identical or opposite absolute configuration, namely L-dimethyl tartrate:L-diisopropyl tartrate: Na⁺ (LmtLiptNa⁺) and L-dimethyl tartrate:D-diisopropyl tartrate:Na⁺ (LmtDiptNa⁺). To this end, we resort to

collision-induced dissociation experiments as well as vibrational spectroscopy as obtained by IRMPD, coupled to quantum chemical calculations. The aim of this work is to assess whether exchange between alkali ion and proton is the only possibility that explains homochiral preference in the mass spectrum of alkali-ion core dimer of dimethyl tartrate or if structural differences between homo and heterochiral complexes could play a role.

Material and methods

I. Experimental Methods

The multistage mass spectrometry (MS^n) experiments were based on a modified Paul ion trap (Bruker, Esquire 3000+). Details of the experiments based on the Paul ion trap can be found elsewhere and only parameters specific to the present study are given below.³⁶ Ions were generated by electrospraying a solution of L tartaric acid dimethyl ester and L or D tartaric acid diisopropyl ester in a 50:50 water/methanol mixture. The concentration was 10^{-5} M for the monomers or the dimers made from a single molecule. A concentration ratio of 1:10 between diisopropyl- and dimethyl ester of tartaric acid was used for studying the mixed dimer. No sodium salt was added to that naturally present as an impurity in the solution. The electrospray ionization (ESI) conditions were as follows: flow rate of 150 μ L/h, drying gas flow of 7.5 L/min, nebuliser pressure of 1.9 bar, capillary voltage of -4500 V, and drying gas temperature of 180°C. The trap drive voltage was adjusted to maximise the intensity of the peak due to the sodium core L tartaric acid dimethyl ester / L or D tartaric acid diisopropyl ester complex.

MS^n experiments were carried out using the standard Bruker Esquire Control software. Collision-induced dissociation (CID) spectra were obtained in a MS^2 experiment by mass selection of the parent in a ± 2 Da window. The parent was fragmented in the Paul ion trap by collision with He, applying a radiofrequency (RF) voltage of variable amplitude during 50 ms.

The IRMPD spectra were recorded resorting to a MS^2 scheme involving IR irradiation in the above-mentioned Paul ion trap. A 1.2 mm hole drilled in the ring electrode of the Paul ion trap allows for the optical access to the centre of the trap. The precursor ions were mass selected in a ± 2 Da window and irradiated for 180 ms in the fingerprint region and 1 s in the 3 μ m region. Mass spectra were recorded after 5 accumulations.

The spectra were recorded in the 800-1800 cm^{-1} range using the infrared free electron laser (FEL) at the “Centre Laser Infrarouge d’Orsay CLIO” based on an electron linear accelerator at an electron energy of 44 MeV.³⁷⁻³⁸ The spectral bandwidth was typically 1% of the central wavelength and the power of the order of 0.8 W. The 2800-4000 cm^{-1} range was covered by a table top IR Optical Parametric Oscillator/Amplifier (OPO/OPA) (LaserVision 10 Hz repetition rate, pulses duration 4-6 ns, spectral bandwidth 3 cm^{-1} , IR power of ~ 200 mW). The IR was focused at the centre of the ion trap using a ZnSe lens of 400 mm focal length.

Infrared spectra were obtained by monitoring the fragmentation efficiency $Y = \ln(P/(F+P))$ as a function of the IR wavenumber; with F the sum of the abundances of the fragment ions produced by IRMPD and P that of the parent ion. The ions produced by IRMPD were the same as those detected in the CID spectra. The tartaric esters were purchased from Sigma-Aldrich International GmbH and used without further purification.

II. Theoretical Methods

The potential energy surface of the different systems was extensively explored using the advanced conformational search tool implemented in the Macromodel software included in the Schrödinger 2015-4 suite of programs.³⁹ The exploration was done using either the OPLS2005 or the MMFFs force fields. The “Systematic torsional sampling”, “Mixed Torsional/Low mode sampling” and “Mixed torsional/Large scale Low mode sampling” were used. Several exploration were done, with different starting points, including arbitrary points of the previous exploration. All complexes obtained after these explorations were recalculated at the OPLS2005 level and sorted out by the “Redundant Conformer Elimination tool”, fixing the RMSD at 1.9 Å. At the end of this step, around eighty conformers were kept for each system. Each of them was optimized within the frame of the density functional theory (DFT) at the RI-B97-d/def2-TZVPPD level⁴⁰⁻⁴¹ with the dispersion correction “disp3 bj abc” including three body effects and Becke-Johnson damping.^{40, 42-43} The option “weight derivatives” was used for the harmonic frequencies calculations. The calculated harmonic frequencies were scaled by 0.975 to account for anharmonicity and basis set incompleteness. The vibrational spectra were simulated by convoluting the harmonic frequencies by a Lorentzian line shape (FWHM 10 cm^{-1}). This level of theory was chosen because it has been successfully applied to neutral, protonated, or alkali core clusters of

biomolecules.⁴⁴⁻⁴⁶ All the calculations were done using the Turbomole V6.6 program package.⁴⁷

We will describe the structures using the notation shown in Scheme 1. The complexes are denoted naming the dimethyl L-tartrate (Lmt) first and then the diisopropyl L/D-tartrate (Lipt/Dipt). The OH or CO groups of interest are indexed with Lmt or Lipt/Dipt depending on the subunit they belong to. Scheme 1 presents the molecules in such a way that the ester functions are localised at the top or the bottom of the illustration plane, on the two sides of an imaginary dividing line defining two half spaces, called 1 and 2. The oxygen atoms of interest are denoted by 1 and 2 for those above and below the dividing line, respectively. For the sake of clarity, Na⁺ is located in subspace 1, *i.e.* above the dividing line, in all the molecular structures shown. The carbonyl and the hydroxyl groups of Lmt located above the dividing line, *i.e.* interacting with Na⁺, are denoted as CO_{Lmt1} and OH_{Lmt1}. Those below the Na⁺ are denoted as CO_{Lmt2} and OH_{Lmt2}. The same notation will be used for the second monomer of the complex replacing Lmt by Lipt or Dipt, which gives CO_{Lipt1}, OH_{Lipt1}, OH_{Lipt2} and CO_{Lipt2}. If the 1 vs. 2 notation is ambiguous, CO_{Lipt1} is the CO interacting with Na⁺ and not hydrogen bonded.

Results and Discussion

III. Experimental results

III 1. Mass spectrum

The mass spectrum (MS) of an electrosprayed solution of Lmt and Lipt, in a concentration ratio of 10:1, is shown in Figure 1. This concentration ratio was chosen because it gives the strongest contribution of mixed sodium-core dimer. Despite the larger concentration of Lmt, the most intense peaks in the MS are due to LiptH⁺ at m/z 235, LiptNa⁺ at m/z 257, and Lipt₂Na⁺ at m/z 491, pointing at a larger proton affinity and a larger cation affinity of Lipt. The complexes involving Lmt, *i.e.* LmtH⁺ at m/z 179, LmtNa⁺ at m/z 201, and Lmt₂Na⁺ at m/z 379, are 5 to 10 times less intense than those involving Lipt. The mixed dimers LmtLiptNa⁺ are observed at m/z 435. The protonated dimers are not observed. In contrast to previous work, where chirality effects were studied by comparing isotopically labelled enantiomers, the analysis of the peaks intensity in the Paul trap is complicated by the fact that Lmt and

Lipt do not have the same affinity for sodium. Still, no chirality effect is observed and the mass spectrum of a solution of Lmt and Dipt is similar to that of a solution of Lmt and Lipt.

III 2. Collision-induced dissociation

The CID spectra of the homochiral LmtLiptNa⁺ and heterochiral LmtDiptNa⁺ sodium-core dimers are shown in Figure 2. The unique fragments are LmtNa⁺ at m/z 201 and LiptNa⁺ or DiptNa⁺ at m/z 257. LiptNa⁺ or DiptNa⁺ is much more abundant as a fragment (\sim x 20) than LmtNa⁺. This is reminiscent of what was observed in the mass spectrum and we can conclude that the preference for Lipt or Dipt also manifests itself in the fragmentation pattern. The CID efficiency is the same within the error for the two diastereomer complexes, as manifested by identical relative intensities of the parent and daughter ion peaks in the two CID spectra.

III 3. IRMPD spectra

The experimental IRMPD spectra of the homochiral LmtLiptNa⁺ and heterochiral LmtDiptNa⁺ sodium-core dimers are shown in Figures 3 and 4, for the fingerprint and the 3 μ m regions, respectively. They are identical whether recorded in a modified hybrid Fourier transform ion-cyclotron resonance (FT-ICR) tandem mass spectrometer (Apex-Qe Bruker Daltonics), equipped with a 7.0 T actively shielded magnet,⁴⁸ or in the quadrupole ion trap, with however higher average fragmentation efficiency for the experiments performed in the FT-ICR (see Figure S1 of the supplementary information). The fingerprint region is characterised by three intense features, located at 1100, 1250, and 1750 cm^{-1} . They appear in the region of the OH bending, CH bending, and CO stretching modes, respectively. The fingerprint region is identical for the homochiral and heterochiral complexes. The hydride stretch region is characterised by a doublet in the region of the free OH stretch, at 3642/3650 cm^{-1} , as well as a broad absorption peaking at \sim 3500 cm^{-1} , typical of one or several bound OH stretches.^{22, 49} The broad absorption band is composed of a single broad band for the heterochiral complex while it displays a shoulder in its high-energy side for the homochiral complex. Also, the ratio between the relative intensity of the doublet relative to the broad absorption is larger (\sim 2) for the heterochiral than the homochiral (\sim 1.3).

IV. Theoretical results

The calculated structures can be classified according to their interaction pattern. The interactions are ionic $\text{Na}^+\dots\text{OC}$ or $\text{Na}^+\dots\text{OH}$ interactions and intermolecular or intramolecular $\text{OH}\dots\text{OC}$ or $\text{OH}\dots\text{OH}$ hydrogen bonds. As will be discussed later on in the assignment, the most stable calculated structures do not reproduce the experimental spectrum. In what follows, we shall therefore briefly describe the most stable structure for both homochiral LmtLiptNa^+ and heterochiral LmtDiptNa^+ complexes, then those to which the experiment is assigned. The xyz coordinates of all the discussed structures can be found in the Supplementary Information Section.

IV 1. Homochiral complex

The most stable homochiral complex, denoted LL hereafter, is shown in Figure 5. None of the intramolecular hydrogen bonds of the sub-units is preserved in LL. Instead, two intermolecular hydrogen bonds take place, namely, $\text{OH}_{\text{Lmt2}}\dots\text{OC}_{\text{Lipt2}}$ and $\text{OH}_{\text{Lipt2}}\dots\text{OC}_{\text{Lmt2}}$. The pattern defined by OH_{Lmt2} , CO_{Lipt2} , OH_{Lipt2} , and CO_{Lmt2} , is strongly non-planar (dihedral angle of 62°). Na^+ interacts with OH_{Lmt2} and OH_{Lipt2} involved in the double hydrogen bond pattern, as well as with the four other polar groups, namely, OH_{Lmt1} , OH_{Lipt1} , CO_{Lmt1} and CO_{Lipt1} . This structure therefore involves interaction between Na^+ and all the polar groups but CO_{Lmt2} and CO_{Lipt2} . The interactions are equally spread between the two subunits, with a symmetrical pattern. The $\text{Na}^+\dots\text{O}$ average distance is 2.90 \AA if one considers all the oxygen atoms, and 2.53 \AA if one considers only the six interacting polar groups.

The complex reproducing the experimental findings will be called LL' in what follows. It is shown in Figure 5. In contrast to LL, it shows only one intermolecular hydrogen bond, $\text{OH}_{\text{Lipt2}}\dots\text{OC}_{\text{Lmt2}}$, accompanied by an intramolecular $\text{OH}_{\text{Lmt2}}\dots\text{OC}_{\text{Lmt2}}$ interaction. Like in LL, six polar groups interact with Na^+ , but they differ in the two dimers: a $\text{Na}^+\dots\text{OC}_{\text{Lipt2}}$ interaction in LL' replaces the $\text{Na}^+\dots\text{OH}_{\text{Lipt1}}$ in LL. As a result, the interaction pattern in LL' is much less symmetrical than in LL. The $\text{Na}^+\dots\text{OC}$ distance is smaller by 0.2 \AA for CO_{Lipt1} than CO_{Lmt1} in LL' while the two distances were almost identical in LL. The $\text{Na}^+\dots\text{O}$ average distance is 3.02 \AA if one considers all the oxygen atoms, and 2.53 \AA if one considers only the six interacting polar groups. The Lipt geometry is very different from that adopted in LL ($\text{HO}_{\text{Lipt1}}\text{-C-C-OH}_{\text{Lipt2}}$ dihedral angle of 180° vs. 0° in the most stable structure).

IV 2. Heterochiral complex

The most stable heterochiral complex, called LD in what follows, is shown in Figure 5. Like in LL, two intermolecular hydrogen bonds take place. However, it does not involve the same polar groups and correspond to $\text{OH}_{\text{Lmt2}} \dots \text{OC}_{\text{Dipt2}}$ and $\text{OH}_{\text{Dipt1}} \dots \text{OC}_{\text{Lmt2}}$ interactions. Like in LL, the doubly hydrogen bond pattern in LD is not planar (dihedral angle of 78°). The LD structure involves the same two $\text{Na}^+ \dots \text{OC}$ and four $\text{Na}^+ \dots \text{OH}$ interactions as LL. The $\text{Na}^+ \dots \text{O}$ average distance is 2.96 \AA if one considers all the oxygen atoms, and 2.56 \AA if one considers only the six interacting polar groups.

The complex reproducing the experiment, called LD' hereafter, is shown in Figure 5. In LD', like in LL', an intramolecular $\text{OH}_{\text{Lmt2}} \dots \text{CO}_{\text{Lmt2}}$ interaction takes place. The intramolecular hydrogen bond is shorter (2.04 \AA) than in LL' (2.17 \AA). The intermolecular hydrogen bond is less directional than in LL'. It consists indeed in a bifurcated hydrogen bond with OH_{Lmt1} acting as a donor to both OH_{Lmt2} and CO_{Dipt2} , with distances of 2.21 and 2.27 \AA , respectively. Compared to the other complexes described above, LD' stands out by the fact that there are only two interactions between Na^+ and Lmt, namely $\text{Na}^+ \dots \text{OH}_{\text{Lmt1}}$ and $\text{Na}^+ \dots \text{OC}_{\text{Lmt1}}$ and three interactions between Na^+ and Dipt, namely $\text{Na}^+ \dots \text{OH}_{\text{Dipt1}}$ and $\text{Na}^+ \dots \text{OC}_{\text{Dipt1}}$ and $\text{Na}^+ \dots \text{OC}_{\text{Dipt2}}$. The $\text{Na}^+ \dots \text{O}$ average distance is indeed much higher than in the other described structures, 3.45 \AA if one considers all the oxygen atoms. This distance is only 2.45 \AA if one considers only the five interacting polar groups.

IV 3. Assignment

The calculated IR absorption of the most stable sodium core dimers, LL and LD, is shown in Figure 6. Although they satisfactorily match with the experiment in the fingerprint region, these structures do not account for the experimental spectra in the $3 \mu\text{m}$ region. We have therefore examined the spectra of all the calculated structures. It turns out that LL' matches very well with the experimental findings obtained for the homochiral dimer. Still, its Gibbs free energy is 5.3 kcal/mol above the minimum. However, ΔG decreases to 3.7 kcal/mol when adding an aqueous solvent as a continuum. Considering the solvent explicitly should result to further stabilisation of LL' relative to LL as the former possesses one more free OH groups that can interact with the solvent through hydrogen bonding. The results for the

heterochiral sodium-core dimer parallel those for the homochiral one. Although LD' is destabilised relative to LD by 6.3 kcal/mol in the gas phase, inclusion of the solvent as a continuum reduces this gap to 3.3 kcal/mol. Explicit inclusion of the solvent is expected to reduce this gap further due to the larger number of sites capable to interact with the solvent in LD' relative to LD.

IV 4a. Fingerprint region

The fingerprint region is shown in Figure 3. The experimental spectra of the homochiral and heterochiral sodium-core dimers are identical and are accounted for by any of the calculated structures. The intense experimental band, at 1740 cm^{-1} , is readily assigned to the superposition of the CO stretches. The calculated frequencies spread over 40 cm^{-1} , which reflects the different environments of the CO groups. Although, the four CO stretches are slightly coupled, the two lower-energy one are localised on Lmt, the two other ones being on Lipt or Dipt. The $\text{Na}^+\dots\text{OC}$ interaction is purely ionic. Consequently, the corresponding CO stretches are higher in frequency than the hydrogen-bonded CO stretches. The most intense band peaking at $\sim 1270\text{ cm}^{-1}$ is assigned to the superposition of modes involving mixed motions of the four OH bends and CH bends, spreading over $\sim 80\text{ cm}^{-1}$. The lower-energy intense feature at $\sim 1090\text{ cm}^{-1}$ is assigned to mode involving mainly the C-OH stretch coupled to deformations localised on the CH_3 groups. No effect of chirality or conformation is observed in this region. Due to the lack of specificity of the fingerprint region, we will not use it for the assignment.

IV 4b. OH stretch region

The $3\text{ }\mu\text{m}$ region is shown in Figure 4. This spectral range is much more specific than the fingerprint region and the spectral pattern strongly depends on the calculated structure. The spectrum of the LL' calculated structure displays two bands in the region of the free OH stretch, the higher-energy one (3662 cm^{-1}) being localised on OH_{Lmt1} and the other one (3638 cm^{-1}) on OH_{Lipt1} . These two bands match well with the doublet experimentally observed at $3642/3653\text{ cm}^{-1}$. The bound OH stretches are calculated lower in energy. OH_{Lmt2} being involved in a frustrated $\text{OH}\dots\text{OC}$ internal bound is calculated at higher energy (3566 cm^{-1}) and weaker oscillator strength than that localised on OH_{Lipt2} , and involved in an intermolecular H bond, calculated at 3503 cm^{-1} . The strong and broad experimental absorption peaking at

3500 cm^{-1} is therefore assigned to the latter while the shoulder at its high-energy side may be assigned to the former. The spectrum of the heterochiral calculated structure LD' displays two free OH stretches. Comparison with the experimental spectrum allows assigning the lower-energy experimental band to OH_{Lipt1} , which interacts with Na^+ , and the high-energy one to the free OH_{Lipt2} . The broad experimental absorption is assigned to the superposition of two modes involving coupled elongations of OH_{Lmt1} and OH_{Lmt2} . The experimental spectra of the homochiral and heterochiral sodium-core dimers are not very different from each other. The interactions at play are indeed very similar in the two diastereomers. In the two complexes, Na^+ interacts with the same three carbonyls CO_{Lmt1} , $\text{CO}_{\text{L or Dipt1}}$, and $\text{CO}_{\text{L or Dipt2}}$. They differ by the nature and the number of additional interactions with Na^+ . In LL', there are three additional interactions that involve OH_{Lmt2} , OH_{Lmt1} and OH_{Lipt2} . In LD', there are only two additional interactions involving OH_{Lmt1} and OH_{Dipt1} . The homochiral and heterochiral complexes differ therefore by the number of $\text{Na}^+\dots\text{O}$ interactions, six for the homochiral and five for the heterochiral complexes and their hydrogen bonding patterns. In LD', OH_{Lmt1} acts as a donor to OH_{Lmt2} , which in turn is internally bound to CO_{Lmt2} . The cooperative effect reinforces the intramolecular hydrogen bond. As a result, the OH_{Lmt1} and OH_{Lmt2} stretches are coupled and appear in the same region, at $\sim 3500\text{cm}^{-1}$. In LL', such a cooperative effect does not happen and the internally bound OH_{Lmt2} stretch is calculated at higher energy, in the region where the shoulder is experimentally observed.

Due to the complexity and flexibility of the studied system, the proposed assignment is only tentative. However, the qualitative conclusions concerning the number of $\text{Na}^+\dots\text{O}$ interactions, six for the homochiral and five for the heterochiral ion-core dimer, and the strength and the nature of the hydrogen bonds explain the slight spectral difference between the two diastereomers.

It should be stressed here that the energetics calculated in the gas phase is at odds with the experimental results. The most stable sodium-core dimers do not correspond indeed to the experiment and the observed complexes probably reflect, or partially reflect, the energetics in solution. This can result from kinetic trapping of the most stable species in solution. Such an effect has been previously observed for protonated ciprofloxacin or its complexes with monovalent or multivalent metal ions, for which the species accounting for the IRMPD spectrum is not the most stable form.^{50 51} The experimental mass spectra indicate that Na^+

binds to Lipt much more easily than to Lmt. However, the mass spectra also indicate that $\text{Na}^+(\text{Lmt})_2$ is more abundant relative to Na^+Lmt than $\text{Na}^+(\text{Lipt})_2$ relative to Na^+Lipt . This is probably due to the fact that the Lmt concentration is 10 times that of Lipt. However, it is also possible that the sodium core dimers are formed via exchange mechanisms or dissociation from larger aggregates.

Conclusion

The results reported here first underline the importance of the OH stretch region for the assignment of the experimental IRMPD spectrum to calculated structures. If we only considered energetics criteria, favouring the most stable complexes, and the fingerprint region, we would assign the observed spectra to the most stable sodium core dimer. However, the results in the OH stretch region allow ruling them out.

Second, the present study confirms that the formation of the sodium core dimers rests on complex mechanisms, and cannot be interpreted in terms of the most stable gas-phase complex. This is in line with the suggestion of Nicolaev *et al.* that formation of the sodium core dimers involve complex exchange mechanism or fragmentation from larger clusters.³²⁻³³ The chirality effects observed here are moderate, despite the presence of the core ion. First, it stems from the calculations that the major difference between the homo and heterochiral sodium-core dimers is the number of $\text{Na}^+\dots\text{O}$ interactions, six for the homochiral and five for the heterochiral. The hetero- and homochiral sodium-core dimers also differ by the nature of the $\text{OH}\dots\text{O}$ hydrogen bonds. The difference in hydrogen bonding pattern is indeed responsible for the difference in spectral pattern in the OH stretch region. This observation is reminiscent of the hypothesis that the interactions responsible for chiral discrimination are not the strongest ionic interactions but weaker ancillary interactions.²³ Low-temperature experiments would greatly help improve the resolution, which in turn would make the chirality effects more visible.^{22 52-53}

Acknowledgments

We thank Dr J. M. Ortega and the CLIO team for technical assistance. Financial Support from the National FT-ICR network (FR3624 CNRS) for conducting the research is gratefully

acknowledged. We acknowledge the use of the computing center MésoLUM of the LUMAT research federation (FR LUMAT 2764) as well as computer time allowance by DI Univ. Paris-Sud.

References

1. Domon, B.; Aebersold, R. Review - Mass Spectrometry and Protein Analysis. *Science* **2006**, *312* (5771), 212-217.
2. Kasprzyk-Hordern, B.; Kondakal, V. V. R.; Baker, D. R. Enantiomeric Analysis of Drugs of Abuse in Wastewater by Chiral Liquid Chromatography Coupled with Tandem Mass Spectrometry. *Journal of Chromatography A* **2010**, *1217* (27), 4575-4586.
3. Nikolai, L. N.; McClure, E. L.; MacLeod, S. L.; Wong, C. S. Stereoisomer Quantification of the Beta-Blocker Drugs Atenolol, Metoprolol, and Propranolol in Wastewaters by Chiral High-Performance Liquid Chromatography-Tandem Mass Spectrometry. *Journal of Chromatography A* **2006**, *1131* (1-2), 103-109.
4. Dwivedi, P.; Wu, C.; Matz, L. M.; Clowers, B. H.; Siems, W. F.; Hill, H. H. Gas-Phase Chiral Separations by Ion Mobility Spectrometry. *Analytical Chemistry* **2006**, *78* (24), 8200-8206.
5. Mie, A.; Jornten-Karlsson, M.; Axelsson, B. O.; Ray, A.; Reimann, C. T. Enantiomer Separation of Amino Acids by Complexation with Chiral Reference Compounds and High-Field Asymmetric Waveform Ion Mobility Spectrometry: Preliminary Results and Possible Limitations. *Analytical Chemistry* **2007**, *79* (7), 2850-2858.
6. Zehnacker, A. *Chiral Recognition in the Gas Phase*. CRC Press Taylor & Francis Group: Boca Raton, 2010.
7. Sawada, M.; Shizuma, M.; Takai, Y.; Adachi, H.; Takeda, T.; Uchiyama, T. Measurement of Chiral Amino Acid Discrimination by Cyclic Oligosaccharides: A Direct Fab Mass Spectrometric Approach. *Chemical Communications* **1998**, (14), 1453-1454.
8. Speranza, M. Enantioselectivity in Gas-Phase Ion-Molecule Reactions. *International Journal of Mass Spectrometry* **2004**, *232* (3), 277-317.
9. Gal, J. F.; Stone, M.; Lebrilla, C. B. Chiral Recognition of Non-Natural Alpha-Amino Acids. *International Journal of Mass Spectrometry* **2003**, *222* (1-3), 259-267.
10. Liang, Y. J.; Bradshaw, J. S.; Dearden, D. V. The Thermodynamic Basis for Enantiodiscrimination: Gas-Phase Measurement of the Enthalpy and Entropy of Chiral Amine Recognition by Dimethyldiketopyridino-18-Crown-6. *Journal of Physical Chemistry A* **2002**, *106* (42), 9665-9671.
11. Rebrov, O.; Kulyk, K.; Ryding, M.; Thomas, R. D.; Uggerud, E.; Larsson, M. Chirally Sensitive Collision Induced Dissociation of Proton-Bound Diastereomeric Complexes of Tryptophan and 2-Butanol. *Chirality* **2017**, *29* (3-4), 115-119.
12. Atlasevich, N.; Holliday, A. E.; Valentine, S. J.; Clemmer, D. E. Collisional Activation of [14pro+2h](2+) Clusters: Chiral Dependence of Evaporation and Fission Processes. *Journal of Physical Chemistry B* **2012**, *116* (26), 7644-7651.
13. Novara, F. R.; Gruene, P.; Schroeder, D.; Schwarz, H. Generation and Reactivity of Enantiomeric (Binolato)Ni⁺ Complexes with Chiral Secondary Alcohols in the Gas Phase. *Chemistry-a European Journal* **2008**, *14* (19), 5957-5965.

14. Schug, K. A.; Lindner, W. Chiral Molecular Recognition for the Detection and Analysis of Enantiomers by Mass Spectrometric Methods. *Journal of Separation Science* **2005**, *28* (15), 1932-1955.
15. Scuderi, D.; Maitre, P.; Rondino, F.; Le Barbu-Debus, K.; Lepere, V.; Zehnacker-Rentien, A. Chiral Recognition in Cinchona Alkaloid Protonated Dimers: Mass Spectrometry and UV Photodissociation Studies. *Journal of Physical Chemistry A* **2010**, *114* (9), 3306-3312.
16. Sivaleela, T.; Kumar, M. R.; Prabhakar, S.; Bhaskar, G.; Vairamani, M. Chiral Discrimination of Alpha-Amino Acids by DNA Tetranucleotides under Electrospray Ionization Conditions. *Rapid Communications in Mass Spectrometry* **2008**, *22* (2), 204-210.
17. Yao, Z. P.; Wan, T. S. M.; Kwong, K. P.; Che, C. T. Chiral Recognition of Amino Acids by Electrospray Ionisation Mass Spectrometry/Mass Spectrometry. *Chemical Communications* **1999**, *20* (20), 2119-2120.
18. Tao, W. A.; Cooks, R. G. Chiral Analysis by Ms. *Analytical Chemistry* **2003**, *75* (1), 25A-31A.
19. Wu, L. M.; Tao, W. A.; Cooks, R. G. Kinetic Method for the Simultaneous Chiral Analysis of Different Amino Acids in Mixtures. *Journal of Mass Spectrometry* **2003**, *38* (4), 386-393.
20. Sen, A.; Le Barbu-Debus, K.; Scuderi, D.; Zehnacker-Rentien, A. Mass Spectrometry Study and Infrared Spectroscopy of the Complex between Camphor and the Two Enantiomers of Protonated Alanine: The Role of Higher-Energy Conformers in the Enantioselectivity of the Dissociation Rate Constants. *Chirality* **2013**, *25* (8), 436-443.
21. Fujihara, A.; Sato, T.; Hayakawa, S. Enantiomer-Selective Ultraviolet Photolysis of Temperature-Controlled Protonated Tryptophan on a Chiral Crown Ether in the Gas Phase. *Chem. Phys. Lett.* **2014**, *610*, 228-233.
22. Tamura, M.; Sekiguchi, T.; Ishiuchi, S.-I.; Zehnacker-Rentien, A.; Fujii, M. Can the Partial Peptide Sivs of Beta2-Adrenergic Receptor Recognize Chirality of Epinephrine Neurotransmitter? *The journal of physical chemistry letters* **2019**.
23. Scuderi, D.; Le Barbu-Debus, K.; Zehnacker, A. The Role of Weak Hydrogen Bonds in Chiral Recognition. *Physical Chemistry Chemical Physics* **2011**, *13* (40), 17916-17929.
24. Filippi, A.; Frascchetti, C.; Guarcini, L.; Zazza, C.; Ema, T.; Speranza, M. Spectroscopic Discrimination of Diastereomeric Complexes Involving an Axially Chiral Receptor. *Chemphyschem* **2017**, *18* (18), 2475-2481.
25. Filippi, A.; Frascchetti, C.; Piccirillo, S.; Rondino, F.; Botta, B.; D'Acquarica, I.; Calcaterra, A.; Speranza, M. Chirality Effects on the IrmPd Spectra of Basket Resorcinarene/Nucleoside Complexes. *Chemistry-a European Journal* **2012**, *18* (27), 8320-8328.
26. Klyne, J.; Bouchet, A.; Ishiuchi, S.; Fujii, M.; Schneider, M.; Baldauf, C.; Dopfer, O. Probing Chirality Recognition of Protonated Glutamic Acid Dimers by Gas-Phase Vibrational Spectroscopy and First-Principles Simulations. *Physical Chemistry Chemical Physics* **2018**, *20* (45), 28452-28464.
27. Pasteur, L. *Leçons De Chimie Professées En 1860 Par Mm. Pasteur, Cahours, Wurtz, Berthelot, Sainte-Claire Devile, Barral Et Dumas*. Hachette: Paris, 1861.
28. Nakazawa, H.; Yoneda, H. Chromatographic Study of Optical Resolution .2. Separation of Optically-Active Cobalt(III) Complexes Using Potassium Antimony D-Tartrate as Eluent. *Journal of Chromatography* **1978**, *160* (1), 89-99.
29. Wijeratne, A. B.; Schug, K. A. Molecular Recognition Properties of Tartrates and Metal-Tartrates in Solution and Gas Phase. *Journal of Separation Science* **2009**, *32* (10), 1537-1547.
30. Wijeratne, A. B.; Spencer, S. E.; Gracia, J.; Armstrong, D. W.; Schug, K. A. Antimony(III)-D, L-Tartrates Exhibit Proton-Assisted Enantioselective Binding in Solution and in the Gas Phase. *Journal of the American Society for Mass Spectrometry* **2009**, *20* (11), 2100-2105.
31. Fales, H. M.; Wright, G. J. Detection of Chirality with the Chemical Ionization Mass Spectrometer. "Meso" Ions in the Gas Phase. *Journal of the American Chemical Society* **1977**, *99*, 2339.
32. Nikolaev, E. N.; Denisov, E. V.; Rakov, V. S.; Futrell, J. H. Investigation of Dialkyl Tartrate Molecular Recognition in Cluster Ions by Fourier Transform Mass Spectrometry: A Comparison of

Chirality Effects in Gas and Liquid Phases. *International Journal of Mass Spectrometry* **1999**, *182*, 357-368.

33. Denisov, E. V.; Shustryakov, V.; Nikolaev, E. N.; Winkler, F. J.; Medina, R. Ft Icr Investigations of Chiral Supramolecular Propellers of Dialkyltartrate Trimers with Methylammonium Ions. *International Journal of Mass Spectrometry* **1997**, *167*, 259-268.

34. Tonner, R.; Schwerdtfeger, P.; May, A. L.; Steill, J. D.; Berden, G.; Oomens, J.; Campagna, S. R.; Compton, R. N. Stability of Gas-Phase Tartaric Acid Anions Investigated by Quantum Chemistry, Mass Spectrometry, and Infrared Spectroscopy. *Journal of Physical Chemistry A* **2012**, *116* (19), 4789-4800.

35. Fernandes, A. S.; Maitre, P.; Corraera, T. C. Evaluation of the Katsuki-Sharpless Epoxidation Precatalysts by Esi-Ftms, Cid, and IrmPd Spectroscopy. *Journal of Physical Chemistry A* **2019**, *123* (5), 1022-1029.

36. Mac Aleese, L.; Simon, A.; McMahon, T. B.; Ortega, J.-M.; Scuderi, D.; Lemaire, J.; Maître, P. Mid-Ir Spectroscopy of Protonated Leucine Methyl Ester Performed with an Fticr or a Paul Type Ion-Trap. *International Journal of Mass Spectrometry* **2006**, *249-250*, 14-20.

37. Prazeres, R.; Berset, J. M.; Glotin, F.; Jaroszynski, D.; Ortega, J. M. Optical-Performance of the Clio Infrared Fel. *Nuclear Instruments & Methods in Physics Research Section a-Accelerators Spectrometers Detectors and Associated Equipment* **1993**, *331* (1-3), 15-19.

38. Prazeres, R.; Glotin, F.; Insa, C.; Jaroszynski, D. A.; Ortega, J. M. Two-Colour Operation of a Free-Electron Laser and Applications in the Mid-Infrared. *European Physical Journal D* **1998**, *3* (1), 87-93.

39. MacroModel Version 9.8; Ed. Schrödinger, Llc: New York, Ny, 2010. *MacroModel version 9.8; ed. Schrödinger, LLC: New York, NY, 2010* **2010**.

40. Grimme, S. Semiempirical Gga-Type Density Functional Constructed with a Long-Range Dispersion Correction. *Journal of Computational Chemistry* **2006**, *27* (15), 1787-1799.

41. Schäfer, A.; Huber, C.; Ahlrichs, R. Fully Optimized Contracted Gaussian Basis Sets of Triple Zeta Valence Quality for Atoms Li to Kr. *J. Chem. Phys.* **1994**, *100*, 5829.

42. Grimme, S.; Antony, J.; Ehrlich, S.; Krieg, H. A Consistent and Accurate Ab Initio Parametrization of Density Functional Dispersion Correction (Dft-D) for the 94 Elements H-Pu. *Journal of Chemical Physics* **2010**, *132* (15).

43. Grimme, S.; Ehrlich, S.; Goerigk, L. Effect of the Damping Function in Dispersion Corrected Density Functional Theory. *Journal of Computational Chemistry* **2011**, *32* (7), 1456-1465.

44. Biswal, H. S.; Loquais, Y.; Tardivel, B.; Gloaguen, E.; Mons, M. Isolated Monohydrates of a Model Peptide Chain: Effect of a First Water Molecule on the Secondary Structure of a Capped Phenylalanine. *Journal of the American Chemical Society* **2011**, *133* (11), 3931-3942.

45. Altnoeder, J.; Bouchet, A.; Lee, J. J.; Otto, K. E.; Suhm, M. A.; Zehnacker-Rentien, A. Chirality-Dependent Balance between Hydrogen Bonding and London Dispersion in Isolated (+)-1-Indanol Clusters. *Physical Chemistry Chemical Physics* **2013**, *15*, 10167-10180.

46. Semrouni, D.; Clavaguera, C.; Dognon, J. P.; Ohanessian, G. Assessment of Density Functionals for Predicting the Infrared Spectrum of Sodiated Octa-Glycine. *International Journal of Mass Spectrometry* **2010**, *297* (1-3), 152-161.

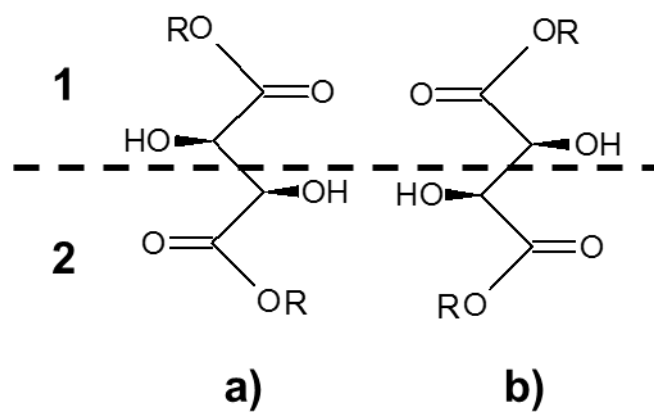
47. Ahlrichs, R.; Bar, M.; Haser, M.; Horn, H.; Kolmel, C. Electronic-Structure Calculations on Workstation Computers - the Program System Turbomole. *Chemical Physics Letters* **1989**, *162* (3), 165-169.

48. Bakker, J. M.; Besson, T.; Lemaire, J.; Scuderi, D.; Maitre, P. Gas-Phase Structure of a Pi-Allyl-Palladium Complex: Efficient Infrared Spectroscopy in a 7 T Fourier Transform Mass Spectrometer. *Journal of Physical Chemistry A* **2007**, *111* (51), 13415-13424.

49. Inokuchi, Y.; Kusaka, R.; Ebata, T.; Boyarkin, O. V.; Rizzo, T. R. Laser Spectroscopic Study of Cold Hostguest Complexes of Crown Ethers in the Gas Phase. *Chemphyschem* **2013**, *14* (4), 649-660.

50. Bodo, E.; Ciavardini, A.; Giardini, A.; Paladini, A.; Piccirillo, S.; Rondino, F.; Scuderi, D. Infrared Multiple Photon Dissociation Spectroscopy of Ciprofloxacin: Investigation of the Protonation Site. *Chemical Physics* **2012**, *398*, 124-128.

51. Piccirillo, S.; Ciavardini, A.; Bodo, E.; Rondino, F.; Scuderi, D.; Steinmetz, V.; Paladini, A. Probing the Competition among Different Coordination Motifs in Metal-Ciprofloxacin Complexes through Irmpd Spectroscopy and Dft Calculations. *Inorganic Chemistry* **2013**, *52* (1), 103-112.
52. Bouchet, A.; Klyne, J.; Ishiuchi, S.; Fujii, M.; Dopfer, O. Conformation of Protonated Glutamic Acid at Room and Cryogenic Temperatures. *Physical Chemistry Chemical Physics* **2017**, *19* (17), 10767-10776.
53. Pino, G. A.; Feraud, G.; Broquier, M.; Gregoire, G.; Soorkia, S.; Dedonder, C.; Jouvet, C. Non-Radiative Processes in Protonated Diazines, Pyrimidine Bases and an Aromatic Azine. *Physical Chemistry Chemical Physics* **2016**, *18* (30), 20126-20134.



Scheme 1

Molecules under study. R=CH₃: dimethyl tartrate; R=C(CH₃)₃: diisopropyl tartrate. a) LL enantiomer (L in short) b) DD enantiomer (D in short)

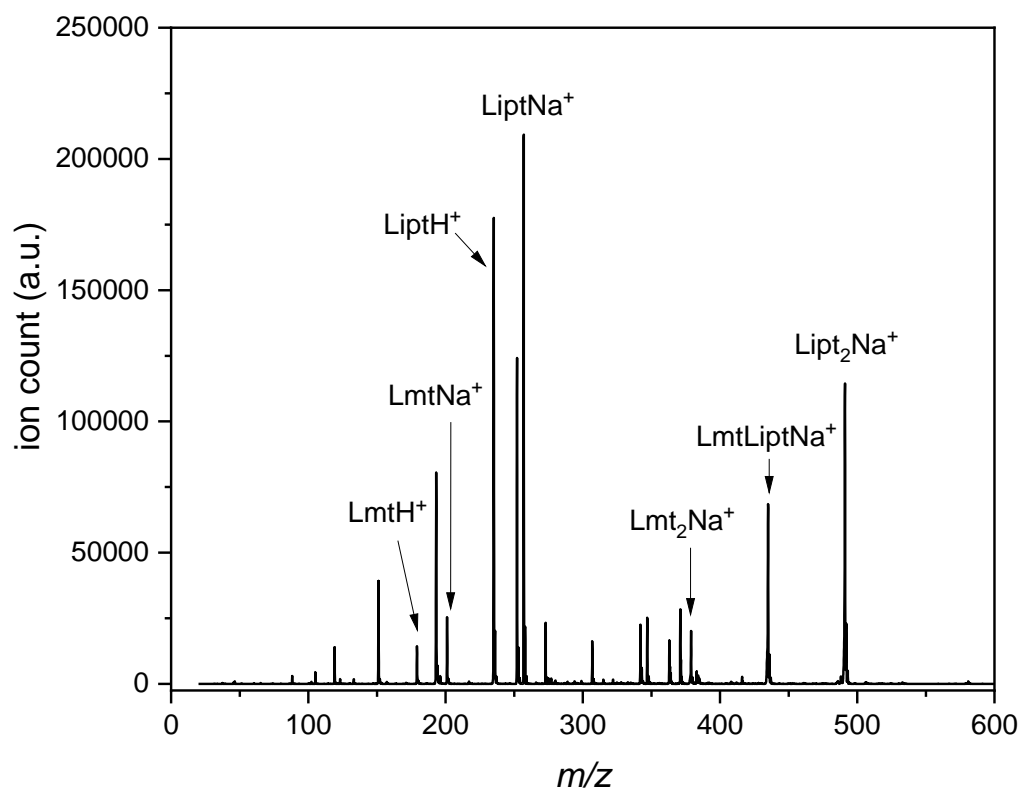


Figure 1

Mass spectrum of an electro sprayed solution of a mixture of Lmt and Lipt in a Paul ion trap, at a concentration ratio of 10:1 (see text). Major cluster ions are indicated in the mass spectrum

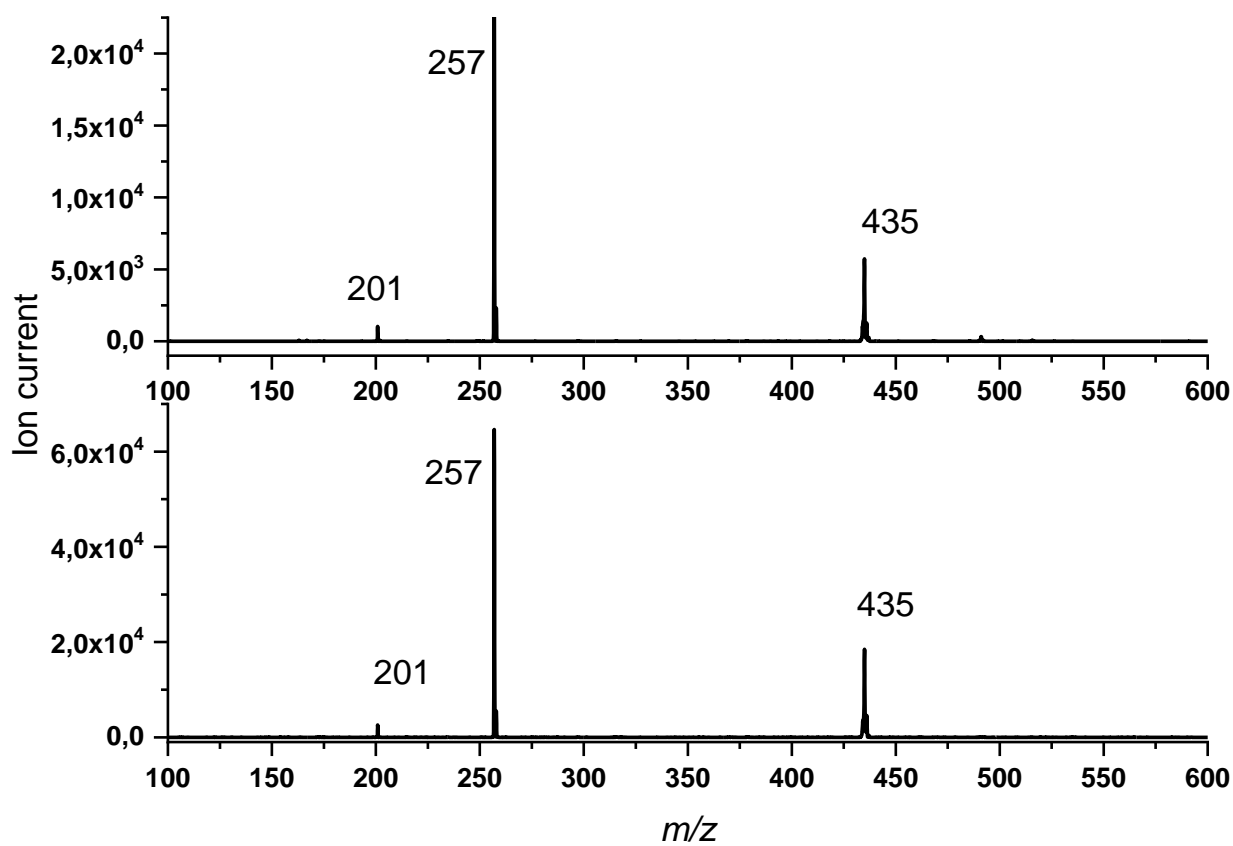


Figure 2

Comparison between CID MS² spectra of the homochiral (top) and heterochiral (bottom) di-methyl tartrate:di-isopropyl tartrate sodium core complex in a Paul ion trap, with RF amplitude of 0.25 V

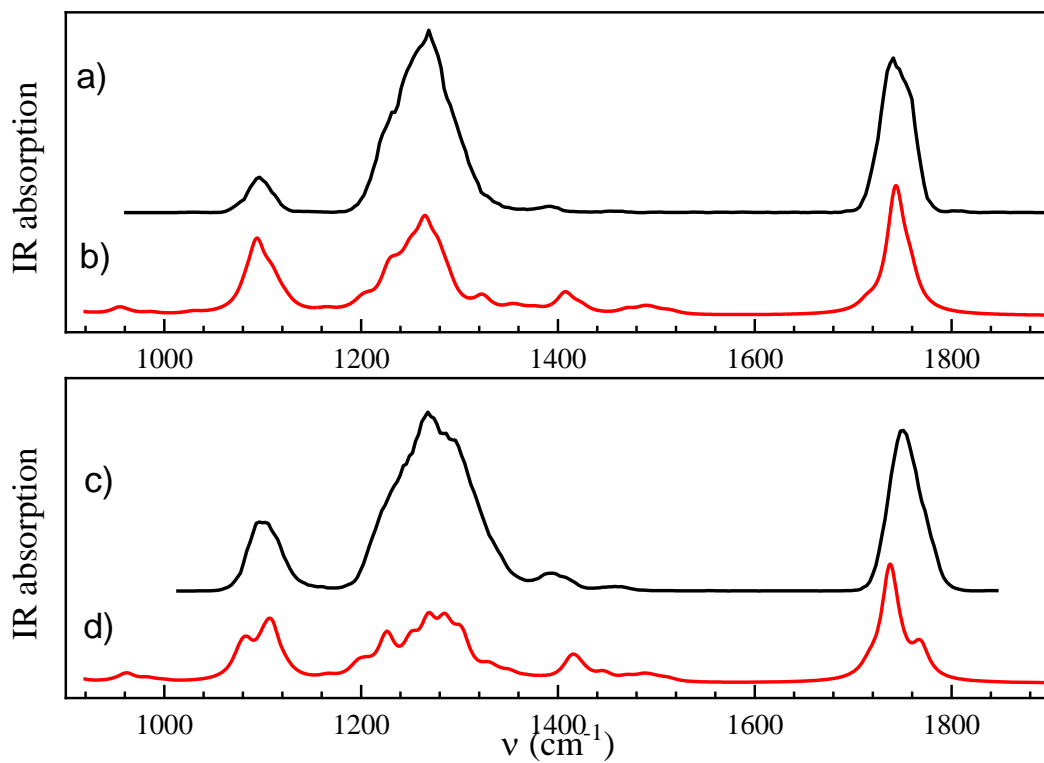


Figure 3

Experimental spectrum in the fingerprint region of a) the homochiral c) the heterochiral di-methyl tartrate : di-isopropyl tartrate sodium-core complex as well as the calculated spectrum of b) LL' and d) LD'

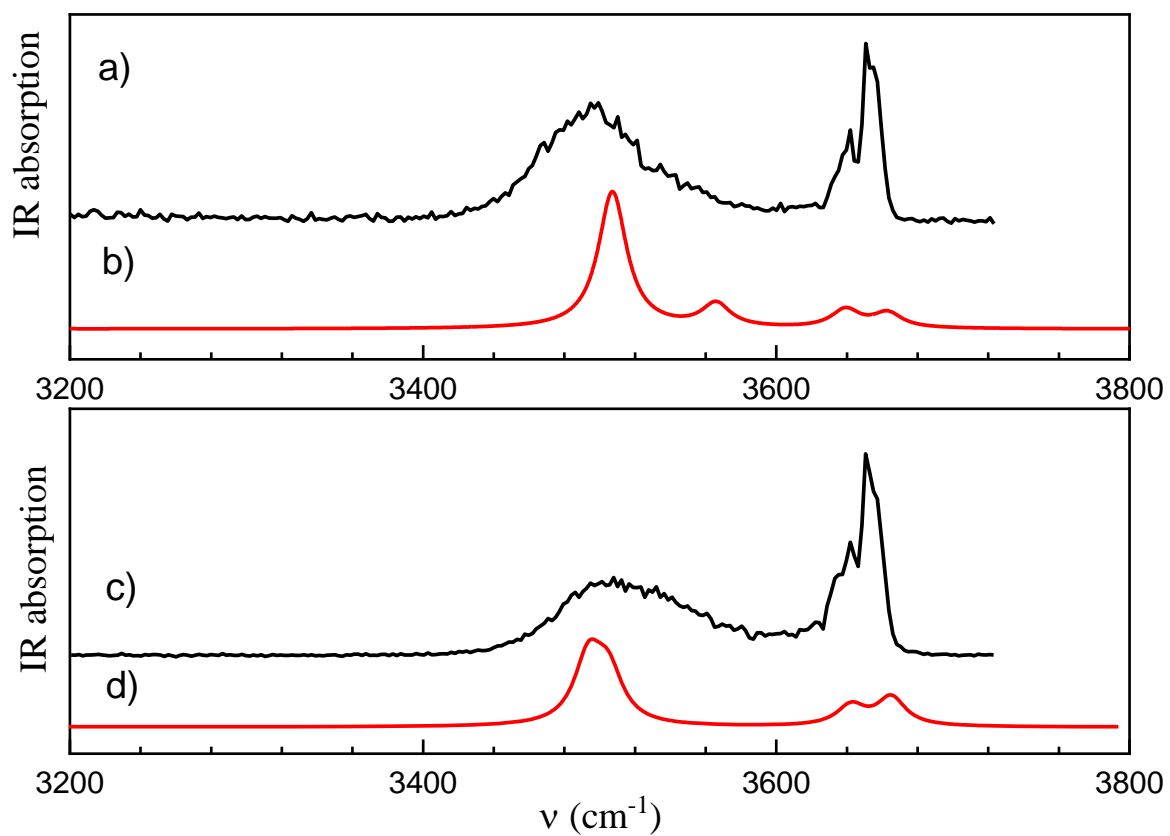
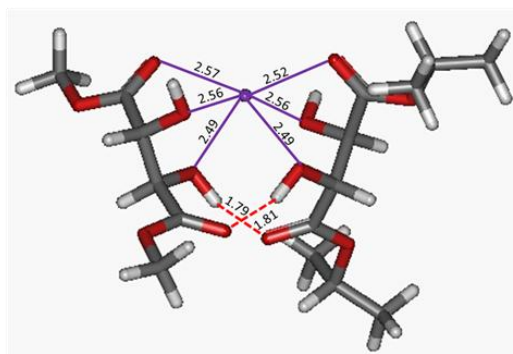


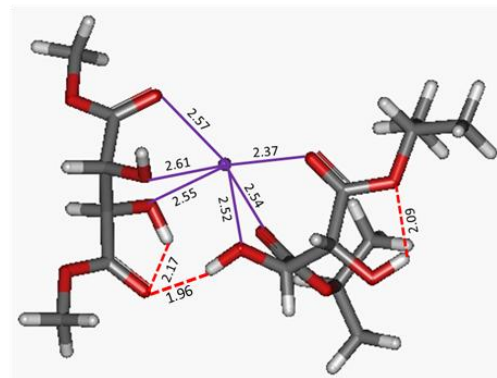
Figure 4

Experimental spectrum in the $3\mu\text{m}$ region of a) the homochiral c) the heterochiral di-methyl tartrate : di-isopropyl tartrate sodium-core complex as well as the calculated spectrum of b) LL' and d) LD'

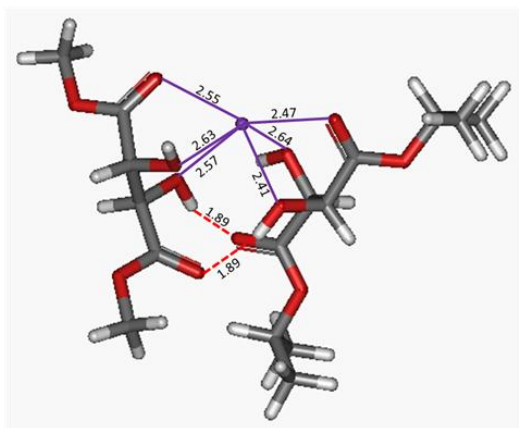
LL : 0.00 kcal/mol



LL' : 5.25 kcal/mol



LD : 0.00 kcal/mol



LD' : 6.31 kcal/mol

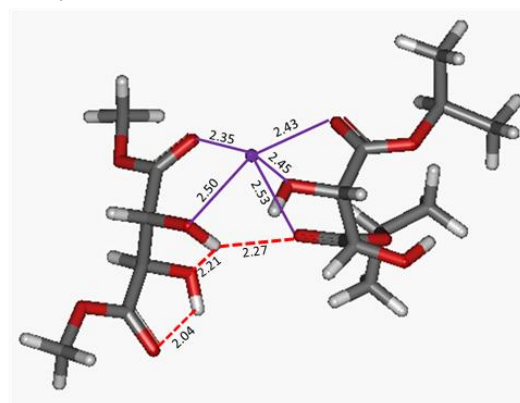


Figure 5

Most stable homochiral complex LL and that assigned to the experiment LL'. Most stable heterochiral complex LD and that assigned to the experiment LD'. The energies are given in vacuum (see text)

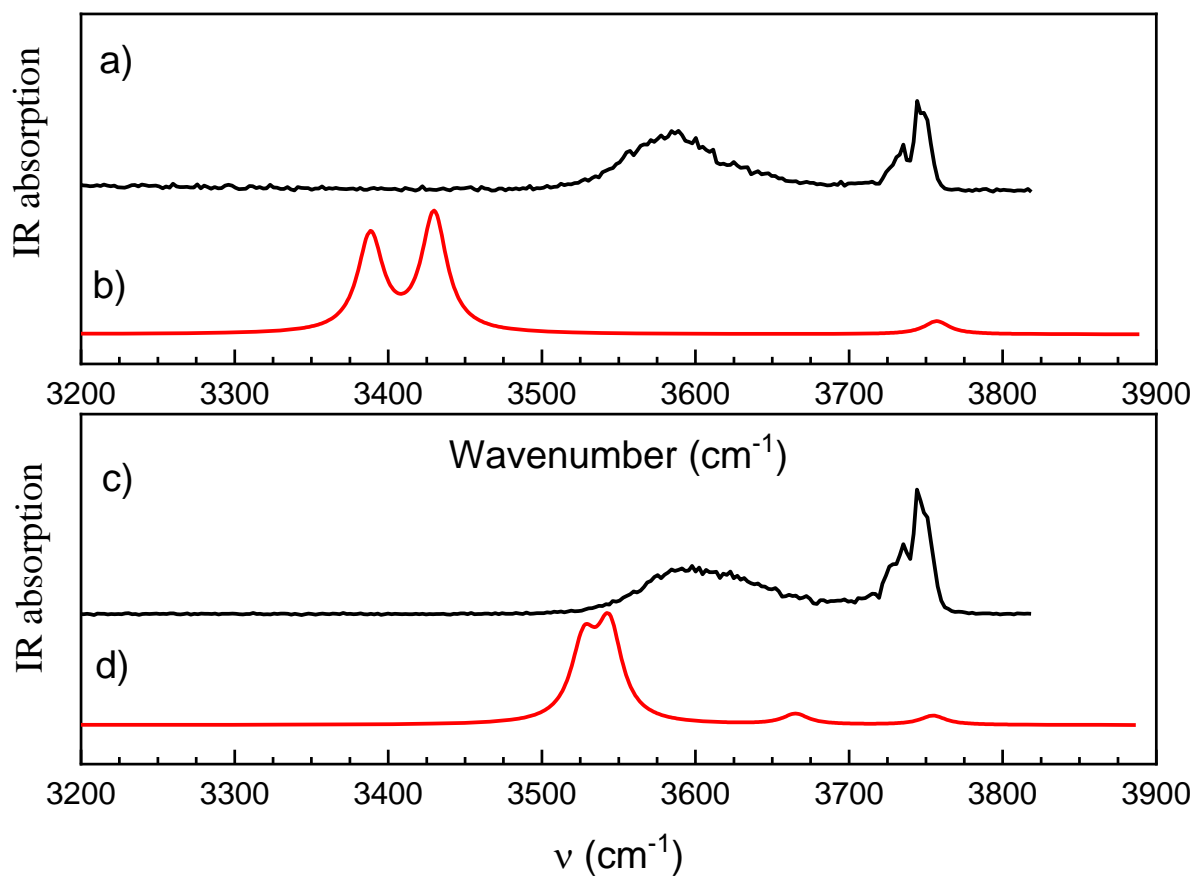


Figure 6

Experimental spectrum in the 3 μm region of a) the homochiral c) the heterochiral di-methyl tartrate : di-isopropyl tartrate sodium core complex as well as the calculated spectrum of b) LL and d) LD